Chapter 5

Self-assembled nanofibers of perylene derivative molecules

3,4,9,10-perylenetetracarboxylic dianhydride (PTCDA) molecules possess a perylene core accompanied with two symmetrical anhydride end groups. This molecule is not only comstructed with hydrocarbon, as the case of coronene molecule, but high electronegative oxygen atoms were also involved. I have utilized the π–π interactions between PTCDA molecules and temperature-induced morphology changes to synthesize 1D nanostructures of PTCDA on a heated (ca. 100 °C) titanium substrate through vacuum sublimation. Because of the pillared Ti structures and the presence of reactive Ti–Cl sites, the titanium substrate played a crucial role in assisting the PTCDA molecules to form 1D nanostructures. The average diameter of the nanofibers deposited on the Ti-CVD substrate at 100 °C was ca. 84 nm, with lengths ranging from 100 nm to 3 μm. When the PTCDA nanofibers were biased under vacuum, the emission current remained stable. The turn-on electric field for producing a current density of 10 μA/cm^2 was 8 V/μm; the maximum emission current density was 1.3 mA/cm^2, measured at 1100 V (E = 11 V/μm). From the slope of the straight line obtained after plotting ln (J/E^2) versus 1/E, I calculated the field enhancement factor β to be ca. 989 cm^{-1}. These results demonstrate the PTCDA nanofibers have great potential for applicability in organic electron-emitting devices.

5.1 Introduction

3,4,9,10-Perylenetetracarboxylic dianhydride (PTCDA) is one of the most intensively studied materials for organic electronic and optoelectonic applications [69, 154].

Investigations into its bulk properties, such as its photoconductivity [155], carrier transport [156], and electroluminescence [96], have led to PTCDA's rapid development for applications in light emitting devices [157], field effect transistors [158], and solar cells [159]. Recently, a number of π-stacking organic molecules, including tris(8-hydroxyquinoine)aluminum [97], (7,7,8,8-tetracyanoquinodimethane)silver [99], coronene [140], anthracene, perylene [98], and copper phthalocyanine [160], have been demonstrated to form one-dimensional (1D) nanostructures readily under lower-temperature conditions than those used typically to prepare analogous structures from inorganic compounds. Moreover, most of these organic 1D nanostructures possess excellent field emission characteristics when biased in a vacuum chamber. Because the morphology of planar π-stacked PTCDA molecules on various substrates can be altered through modification of the processing temperature—i.e., granular morphologies at room temperature, island morphologies at high temperature [33-34, 159–164]—I suspected that PTCDA might form 1D structures under certain conditions. As a matter of fact that Liu et al. have synthesized the PTCDA nanorods by solid-phase reaction [98]. However, in that process, PTCDA molecules react with BaO in a heated quartz tube (280 °C) for 2 hours. Such a high process temperature may not be suitable for certain substrates. For example, the high temperature will deform the glass substrate or diffuse metal atoms into bulk substrate, e.g. silicon substrate, and form a solid solution. Moreover, the nanorods were synthesized on a poor conductive BaO substrate, which is inappropriate to measure the field emission property directly. In this chapter, I present nanofibers having high aspect ratios formed using a relatively low-temperature (100 °C) process and describe the significant effect that the Ti substrate formed by plasma enhancement chemical vapor deposition (PECVD) has on the 1D structural growth. I also evaluate the field emission characteristics of the PTCDA nanofibers synthesized directly on Ti metal films. The results open up an interesting area of study and suggest potential further applications.

5.2 Experimental Section

PTCDA films were grown through vacuum sublimation in a thermal coater at a base pressure of ca. 3×10^{-6} torr. A commercial powders of PTCDA ($C_{24}H_8O_6$; Aldrich) was sublimed onto various substrates, including Ti and Au, from a heated crucible; a crucible

temperature of ca. 100 °C corresponded to a deposition rate of 1 Å/s, as determined using a quartz crystal microbalance. To study the effect that altering the temperature had on the film morphology, the substrate temperature (T_{sub}) was maintained at 25, 80, 100, or 120 °C. The Au substrate was prepared by depositing a Au film on a Si (100) substrate through e-gun evaporation (physical vapor deposition; PVD); I denote this substrate as "Au-PVD". The Ti substrate was prepared by depositing a Ti film on a Si (100) substrate using the PECVD technique; this sample is denoted "Ti-CVD". Details of the PECVD process have been reported elsewhere [165]; it mainly utilizes titanium tetrachloride ($TiCl_4$) to react with H_2 and form a metallic Ti film in a plasma-generating chamber. A Ti substrate deposited using the sputter technique (a variation on PVD) was also prepared to ascertain the effect that the substrate has on forming the PTCDA nanofibers; I denote this substrate as "Ti-PVD."

Structural investigations were performed using a JEOL JSM-6500F scanning electron microscope (SEM). The profiles and fine structures of the nanostructures were imaged and analyzed using a JEOL JEM-2010F high-resolution transmission electron microscope (HRTEM) equipped with an Oxford energy dispersive spectrometer. The substrate morphologies were investigated using a Veeco D5000 atomic force microscope (AFM). The concentration of trace elements was determined using an ATOMIKA TXRF-8030W total reflection X-ray fluorescence (TXRF) spectrometer. The field emission measurements were performed in a vacuum chamber (ca. 10^{-6} torr); a cylindrical copper electrode (diameter: 2.2 mm) was positioned above the substrate surface at a distance of 100 μm. A Keithley 237 instrument was used to measure the emission current of the PTCDA nanofibers as a function of the sweep bias.

5.3 Results and Discussion

PTCDA molecules tend to form island morphologies on various substrates at elevated temperatures [33-34, 159-164]. To determine the growth conditions necessary to prepare PTCDA nanofibers, I deposited PTCDA onto Ti and Au substrates at various temperatures and assessed the film morphologies by means of SEM.

5.3.1 Film morphology

Figures 5-1 (a)–(h) display SEM topographic images of PTCDA films deposited on Au and Ti–CVD substrates under various temperatures. At room temperature, the film morphology on the Au substrate was that of contiguous granular structures having an average grain size of 45 nm [Fig. 5-1 (a)]. As the substrate temperature increased, I observed typical temperature-induced morphological changes [164, 166]; i.e., Figs. 5-1 (b)–(d) indicate that the film morphologies changed from grains to facets and finally to separated islands upon increasing the temperature. According to Krause et al., PTCDA films deposited at room temperature are metastable. When PTCDA is deposited at elevated temperatures, or when PTCDA-coated substrates are annealed at high temperatures, the adsorbate contains a sufficient amount of energy to diffuse to already existing crystallite sites in an energetically favorable process [34, 164]. Such morphological changes may also occur through strain relaxation mechanisms [165]. As a result of strong chemisorption, the first layer of PTCDA is strained, such that the molecules adsorbed onto larger island sites have lower energies than those adsorbed onto smaller island sites; Stranski–Krastanov (SK) growth may help to relax this strain [163, 166]. When the temperature increases, the islands grow at the expense of the number of crystallites, and the space between the islands extends gradually. Moreover, portions of the adsorbate desorb from the substrate, resulting in decreasing island density. Among our SEM images, I also observed needle- and belt-like structures lying on the Au substrate. According to the S-type growth model [161], these structures result from homogeneous nucleation, i.e., the PTCDA molecules combined prior to adsorbing on the substrate. Under these circumstances, the adsorbate formed elongated needles through stacking of additional molecules along the needle's axis.

Figures 5-1 (e)–(h) present the PTCDA film morphologies on the Ti-CVD substrate at the same set of temperatures. In this case, I observed that many more of the needle-like structures existed on the Ti-CVD substrate than they did on the Au substrate. The cause of this change in film morphology was very subtle; I suggest two possibilities. First, according to the film growth mechanism, the adsorbate usually diffuses to the step edges of terraces [143]; thus, the substrate morphology plays an important role as a template. In Fig. 5-1 (e), I observe a preformed 1D nanostructure having a diameter of 30 nm that looks like a string of beads. After examining the morphology of pure Ti-CVD substrate

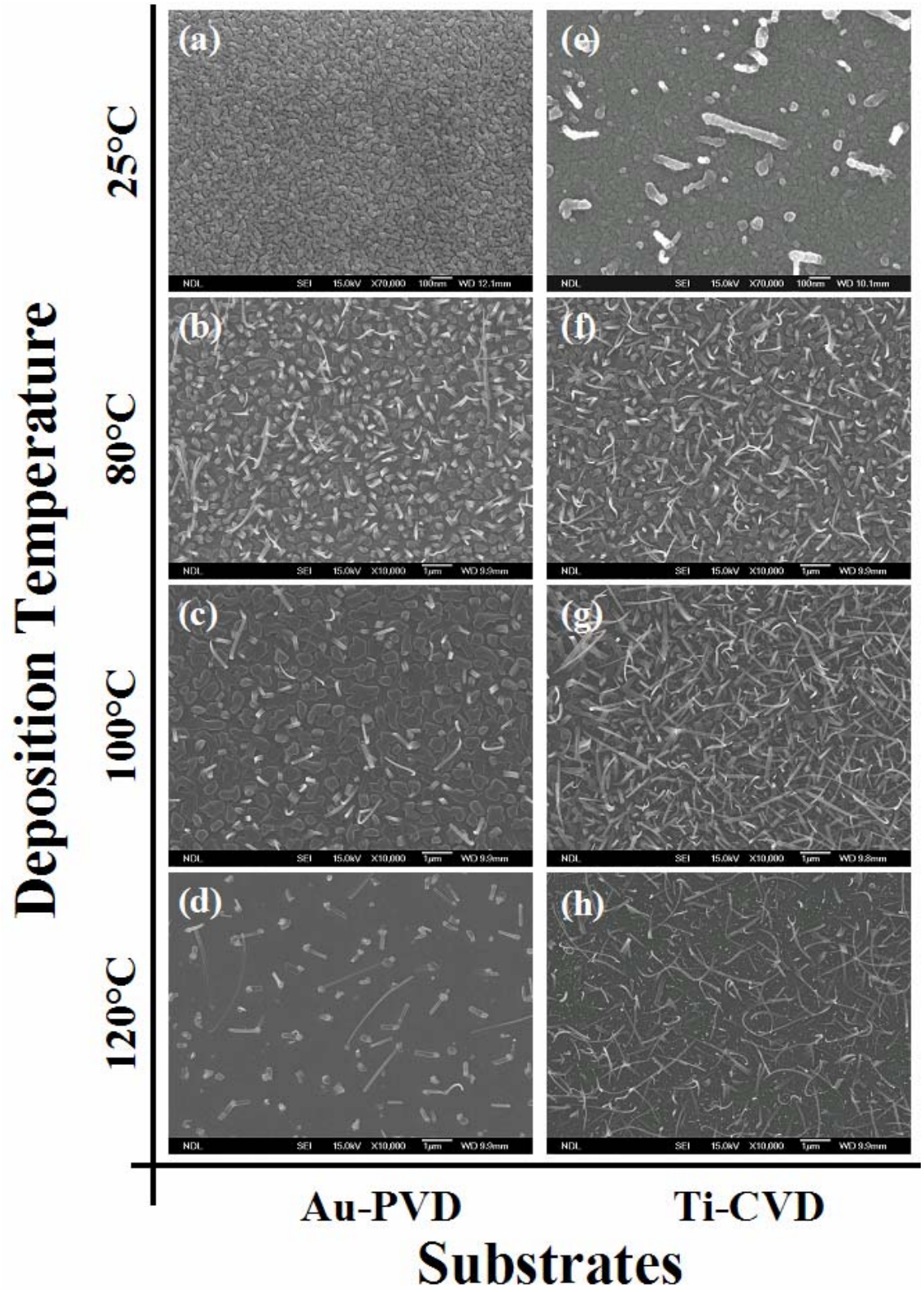

Figure5-1 *Top-view SEM images of PTCDA layers deposited on an Au substrate at values of T_{sub} of (a) 25, (b) 80, (c) 100, and (d) 120 °C and on a Ti substrate at values of T_{sub} of (e) 25, (f) 80, (g) 100, and (h) 120 °C. To discern the subtle difference between samples deposited at room temperature, the images of Figures 5-1 (a) and (e) have been magnified by 70,000 times, whereas the others have been magnified only 10,000 times*

with AFM, I realized that this threaded bead structure existed on the Ti-CVD substrate prior to the formation of the PTCDA film, suggesting that the Ti pillar morphology might induce and enhance the formation of 1D nanostructures of PTCDA. The other possibility is that when the Ti film was deposited using $TiCl_4$ as a liquid source precursor, incompletely reacted $TiCl_4$ probably remained on the Ti film; i.e., some of the Ti surface atoms were still bonded to chlorine atoms. Because $TiCl_4$ and $TiCl_3$ are strongly Lewis acidic (electrophilic) groups [16], such units might provide sites for reacting with PTCDA adsorbate molecules. Table 5-1 displays the trace element concentration of the Ti-CVD substrate, as determined using TXRF spectrometry; indeed, I observe the existence of chlorine atoms on the Ti-CVD substrate (ca. 9 at%). Consequently, when depositing PTCDA at high temperature, the presence of reactive Ti–Cl sites might lead to the preference for deposition of PTCDA and form nanofiber structures.

Comparing Figures 5-1 (d) and (h), which display images of the materials prepared at a temperature at which some of the PTCDA molecules re-evaporated from the substrate (T_{sub} = 120 °C), the number of nanostructures present on the Ti-CVD substrate is greater than that on the Au substrate. I ascribe this phenomenon partly to the dianhydride groups of PTCDA bonding more strongly to the reactive Ti substrate than to the inert Au substrate. This observation is consistent with the UPS results reported by Heroes et al. [167, 168]

5.3.2 Subatrate effect

5.3.2.1 Topography of substrate

To confirm our assumption that the nanofibers formed relatively easier on the Ti-CVD substrate as a result of the substrate template effect operating in conjunction with the presence of reactive Ti–Cl sites, I used PVD to prepare another Ti substrate to compare its behavior with that of the Ti-CVD substrate. The Ti-CVD and Ti-PVD films both exhibited hexagonal structures, as characterized using grazing incident X-ray diffraction (GID). Figures 5-2 (a) and (b) display topographic SEM images of the PTCDA films, which I deposited simultaneously, at a value of T_{sub} of 100 °C, onto both the Ti-CVD and Ti-PVD substrates. These images reveal that the mechanism of nanofiber formation did not depend simply on the intrinsic properties of the Ti substrates. Figures 5-3 (a) and (b) present the initial morphologies of the Ti-CVD and Ti-PVD substrates, respectively, prior to deposition of PTCDA. The image of the Ti-PVD surface indicates that it had a smooth

topography with a root mean square roughness of 1.3 nm, a value that is quite normal for a sputtered metal film. In contrast, the image for the Ti-CVD sample indicates that pillared structures existed, with a root mean square roughness as high as 25.5 nm. Based on the theory that the adsorbate has a greater tendency to diffuse toward and grow along the step edge, I attribute the enhanced growth of the 1D nanostructures on Ti-CVD primarily to its abrupt pillar-shaped morphology. When I deposited PTCDA on the heated Ti-CVD substrate, the mobile adsorbate molecules shifted location to the vicinity of the Ti pillars and grew around them.

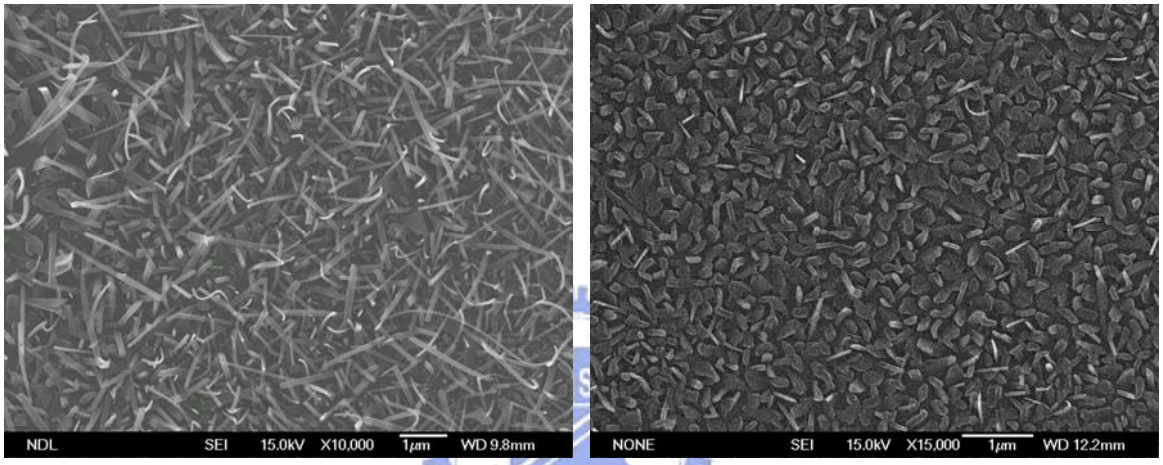

Figure 5-2 *Top-view SEM images of PTCDA layers deposited on (a) Ti-CVD and (b) Ti-PVD at values of T_{sub} of 100 °C.*

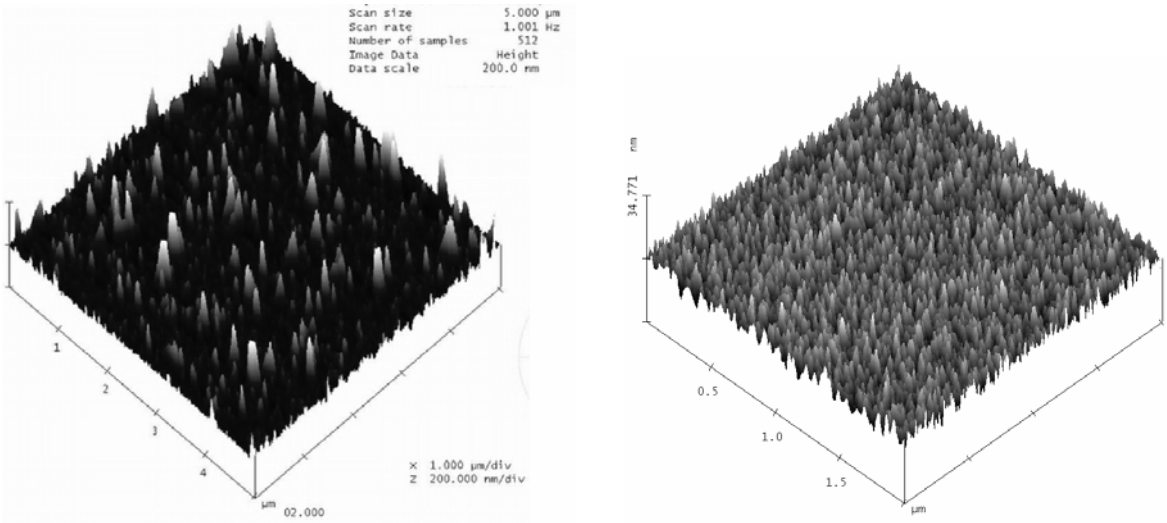

Figure 5-3 *AFM images of the (a) Ti-CVD (image area: 5 × 5 μm^2; height: 200 nm) and (b) Ti-PVD (image area: 2 × 2 μm^2; height: 34.77 nm) substrates.*

5.3.2.2 Reactive sites of substrate

The results of the TXRF analyses for both substrates (Table 5-1) further support our hypotheses. Although I detected chlorine atoms (ca. 9 at.%) on the Ti-CVD substrate, none could be detected on the Ti-PVD substrate. As mentioned previously, $TiCl_x$ species are highly reactive Lewis acids—for example, some are used as Ziegler–Natta catalysts for olefin polymerization [169]; if the reactive Ti–Cl sites of our substrate act as anchor sites of the first set of deposited PTCDA molecules, subsequent molecules will deposit upon them through π–π interactions to develop 1D nanostructures.

Table 5-1 *The concentration of trace elements on Ti-CVD substrate and Ti-PVD substrate.*

Element	Ti-CVD substrate Concentration ± sigma [10^{10} Atoms/cm^2]	Ti-PVD substrate Concentration ± sigma [10^{10} Atoms/cm^2]
Ti	673940.55 ± 6619.29	255681.04 ± 2469.12
Cl	60211.44 ± 700.33	Not detected

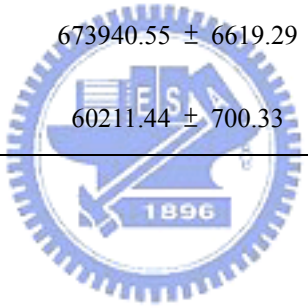

5.3.3 HRTEM

Figure 5-4 (a) presents an HRTEM image of a single PTCDA nanofiber, having a diameter of 22 nm, that was formed at a value of T_{sub} of 100 °C on the Ti-CVD substrate. In Figure 5-4 (b), the high-magnification image displays fringes that are orientated in short-range order at the edges of the nanofiber, but entangled randomly within the nanofiber. The electron diffraction pattern presented in the inset of Figure 5-4 (a) displays only amorphous rings, rather than distinct diffractive spots, suggesting an insignificant degree of crystallinity. In addition, I did not observe any catalyst at the tip of the fiber, similar with previous results of other organic nanofibers [140, 34]. Therefore, the growth mechanism is dissimilar to that of carbon nanotubes (CNTs), which require a catalyst surface to enhance the decomposition of the hydrocarbon reactants, forming a supersaturated solution of carbon and catalyst, which finally precipitates carbon atoms and extrudes the walls [118].

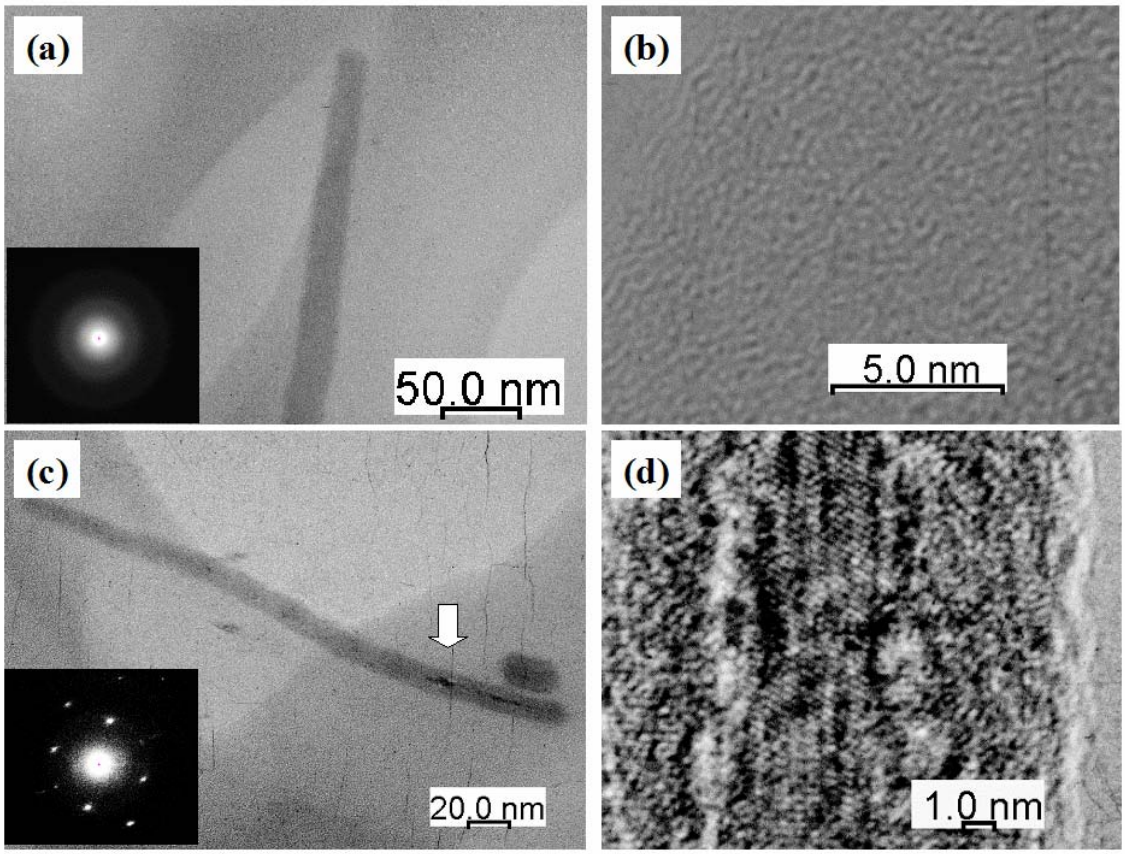

Figure 5-4 *(a) HRTEM image of a single PTCDA nanofiber formed on the Ti-CVD substrate at a value of T_{sub} of 100 °C. Inset: The corresponding electron diffraction pattern. (b) A magnified image of the nanofiber in (a), displaying its amorphous structure. (c) HRTEM image of a single Ti-included PTCDA nanofiber (diameter: 12 nm). The corresponding electron diffraction pattern in the inset displays Ti atoms within the fiber. (d) Magnified image of the nanofiber in (c), high-lighting the heterogeneous region, which exhibits a crystallized structure.*

Interestingly, although most of the PTCDA nanofibers were amorphous and included no catalyst, certain nanofibers did contain titanium atoms within them. Figure 5-4 (c) presents an image of a PTCDA nanofiber having a diameter of ca. 12 nm. This nanofiber possessed a heterogeneous structure, as indicated by the arrow. When selected area diffraction (SAD) was performed, a distinct diffraction pattern was observed, as shown in the inset of Figure 5-4 (c). I examined this heterogeneous structure further through the use of energy dispersive spectroscopy (EDS), with which I found peaks associated with Ti atoms. Figure 5-4 (d) presents a magnified image of the heterogeneous structure; I observe Ti atoms arranged in an ordered manner within the nanofiber, accompanied by

amorphous carbon atoms located around the outer region. This observation further supports our mechanism for the growth of PTCDA nanofibers. Parts of the PTCDA nanostructure grew along the Ti pillars and, in some cases, they grew around these pillars. The highly electronegative chlorine atoms on the Ti surface attract electrons and weaken the bonding between Ti atoms; consequently, some of the chlorine-bound Ti atoms ($TiCl_x$) might desorb from the surface at high temperature. Because Ti atoms have a great tendency to react with the anhydride groups of PTCDA [167], desorbed $TiCl_x$ species might react with incoming PTCDA adsorbate units to form Ti-included PTCDA nanofibers.

5.3.4 Exterior of PTCDA nanofibers

Figure 5-5 presents side-view SEM images of the PTCDA nanofibers deposited on the Ti-CVD substrate at a value of T_{sub} of 100 °C. The average diameter of these nanofibers was ca. 84 nm, with lengths ranging from 100 nm to 3 μm. The nanofibers stand with angles on the Ti substrate as a result of repulsive forces among nuclei, which led to a parallel-displaced conformation and resulted in tilted columnar structures [15].

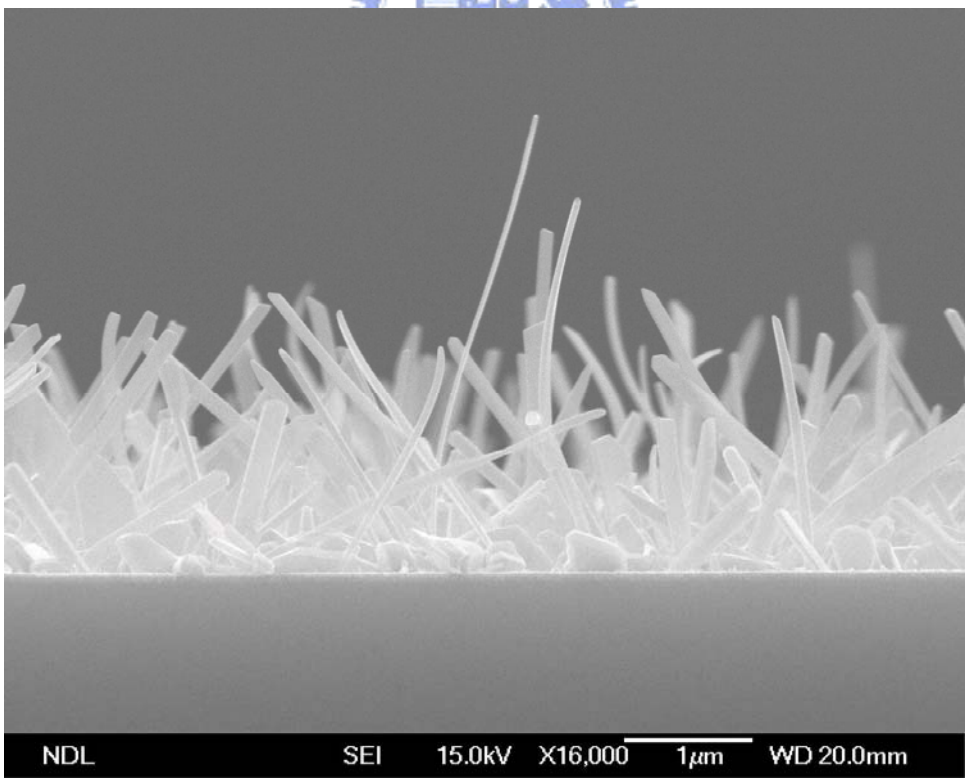

Figure 5-5 *Side-view SEM images of PTCDA nanofibers deposited on the Ti-CVD substrate at a value of T_{sub} of 100 °C.*

5.3.5 Field emission of PTCDA nanofibers film

Field emission characterization of the PTCDA nanofibers synthesized on a heated (100 °C) Ti-CVD substrate was performed under vacuum (5×10^{-6} torr) by placing a cylindrical Cu electrode (diameter: 2.2 mm) at a distance of 100 μm above the surface of the sample. The Cu electrode was connected to the source monitor unit (SMU) of a Keithley 237 instrument, and the titanium substrate beneath the PTCDA nanofibers was grounded. Figure 5-6 presents the emission current density (J) as a function of the applied field (E). The turn-on field required for the PTCDA nanofibers to produce a current density of 10 μA/cm^2 was 8 V/μm; the maximum emission current density of 1.3 mA/cm^2 occurred at a potential of 1100 V (E = 11 V/μm). This performance is better than that of the CuPc nanofibers discussed in chapter 4. From the point of view of electron injection, the electron affinity (4.6 eV) of PTCDA [170] is close to the work function (4.33 eV) of the Ti substrate [171]; thus, electrons are able to transfer from the Ti substrate to the PTCDA nanofibers much more readily than they could from an Au substrate (5.1 eV) to CuPc nanofibers (3.1 eV). Furthermore, the strong bonding between the Ti substrate and the dianhydride groups of PTCDA molecules provides a better interface for electron injection [167].

The Fowler–Nordheim (FN) theory is most commonly used to model the emission of cold electrons from a conductor under a strong field [104]. By plotting ln (J/E^2) versus 1/E, one can obtain a straight line, the slope of which can be used to deduce the field enhancement factor (β) [105]. The inset of Figure 5-6 indicates that the plot of ln (J/E^2) versus 1/E is a straight line, implying that the field emission from these nanofibers follows FN theory. From the values of the work function of bulk PTCDA (4.6 eV) and the slope of the fitted line (–64.21), I calculated the field enhancement factor β of the PTCDA nanofibers to be 989 cm^{-1}. This value is smaller than determined for a CNT film (1000–3000 cm^{-1} for a 125-μm inter-electrode distance) [172], presumably because of the different length-to-radius (L/r) ratios of the 1D nanostructure, as has been discussed elsewhere [97]. As compared with similar π-stacked organic 1D nanostructure, AlQ_3 nanowires, the field enhancement factor of the PTCDA nanofibers is higher than the value of AlQ_3 nanowires (β = 275 cm^{-1}) [97]. Although the L/r ratio of the AlQ_3 nanowires (L/r = 5.5 μm/20 nm = 275) was higher than that of the PTCDA nanofibers (L/r = 2.2 μm/84 nm = 26), the lower work function of AlQ_3 (3.0 eV) relative to that of PTCDA (4.6 eV)

limits the deduced value of according to the formula $\beta = B\phi^{3/2} / slope$, where $B = 6.83 \times 10^9$ V m^{-1} eV$^{-3/2}$ [159, 105]. This result reveals that the geometric shape and intrinsic properties of the emitter both influence the field enhancement effect.

Figure 5-7 displays the emission current stability of the PTCDA nanofibers when biased at 1000 V (E = 10 V/μm) for 1600 s. The mean current density was ca. 0.5 mA/cm^2 with a perturbation of less than one order of magnitude. The field emission current did not decay during the stability measurements, demonstrating that the PTCDA organic nanofibers is suitable for applications as electron emitting devices.

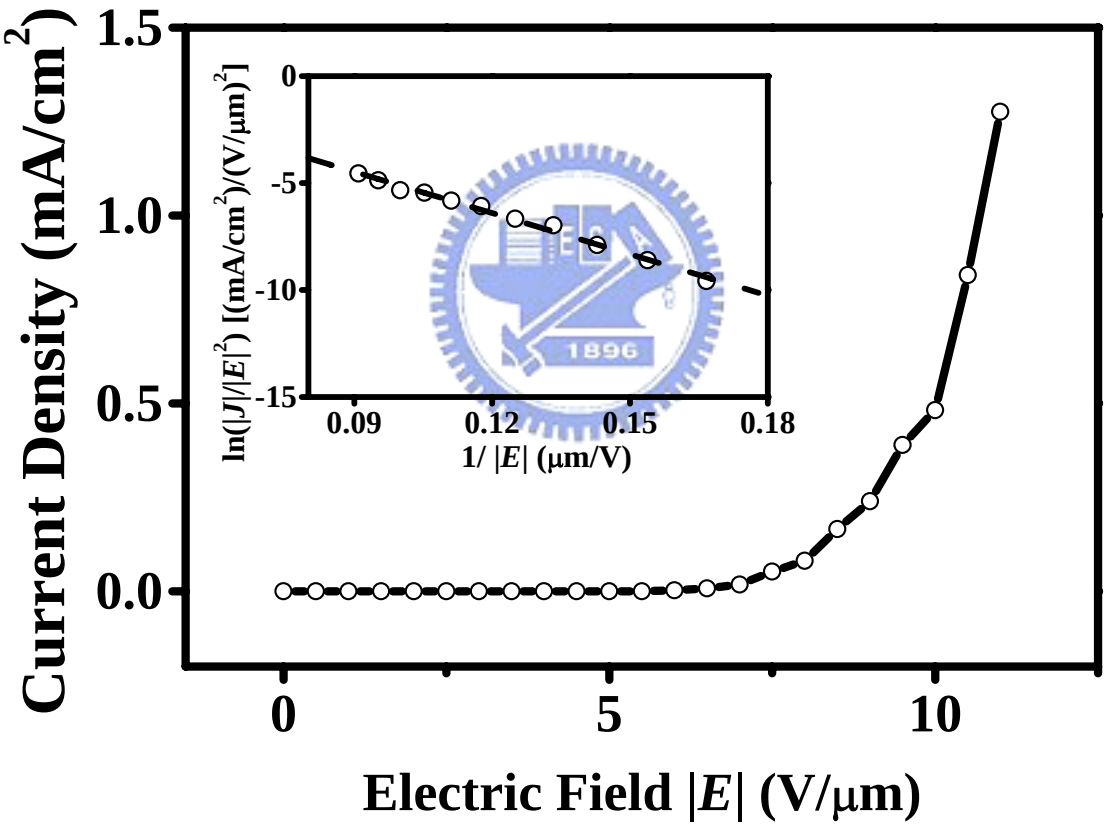

Figure 5-6 *Field emission J–E curve of the PTCDA nanofibers. Inset: Corresponding FN plot.*

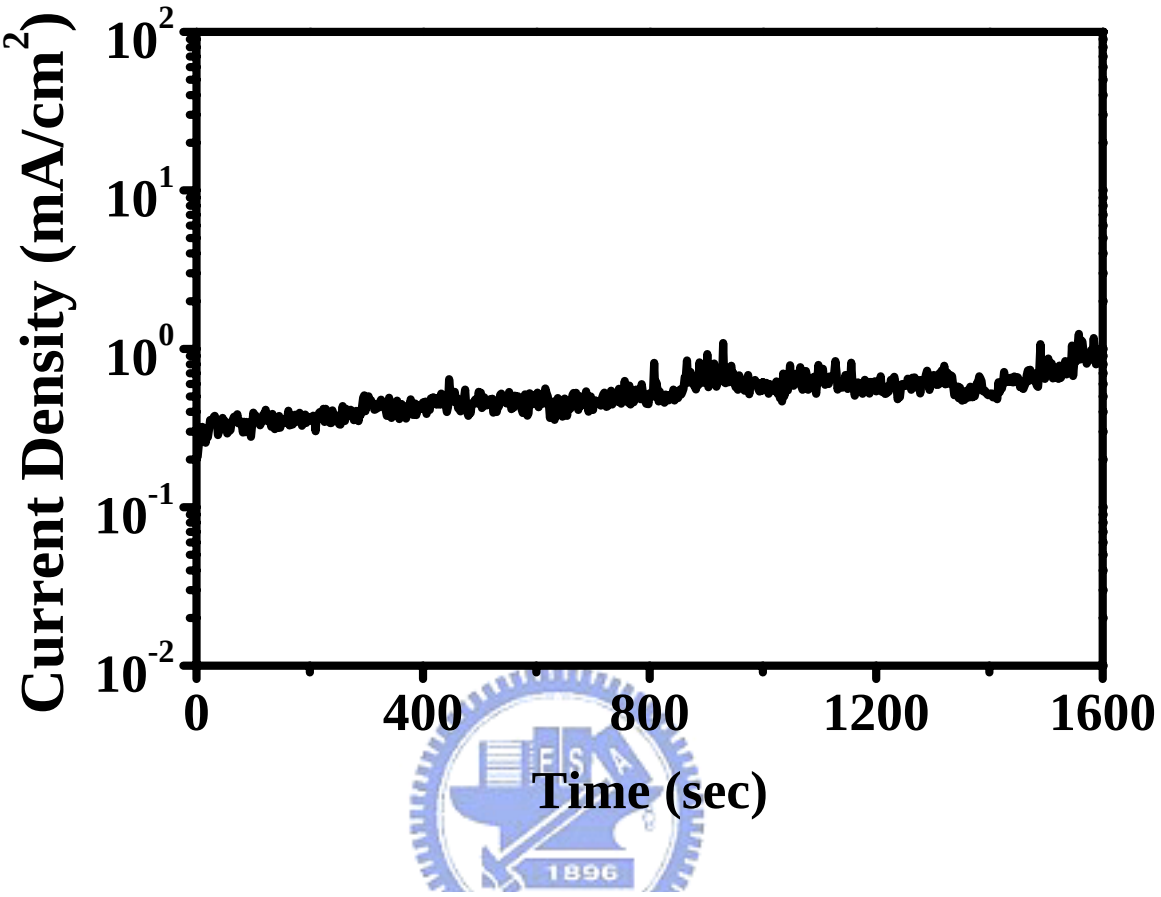

Figure 5-7 *Emission current of the PTCDA nanofibers plotted at a constant voltage.*

5.3.6 Field emission of single PTCDA nanofiber

As the experiment I discussed in section 3.3.5, I utilized the vacuum emission current measurement system assembled in SEM instrument to insure that the emission current was contributed by the PTCDA nanofiber. By keeping tungsten probe at a distance of 300 nm above a PTCDA nanofiber as shown in Figure 5-8, the field emission current was measured and plotted in Figure 5-9. Owing to the tip radius of tungsten probe is around 145 nm, a value that is smaller than the space between two individual fibers, I can evaluate the field emission characteristic of single individual nanofiber without the interference of electrostatic shielding effect caused by other neighboring fibers. The turning point of the curve for producing a current of 1 nA was near 142 V, and beyond 180 V, the emission current reach the maximum current limit of the measuring tool.

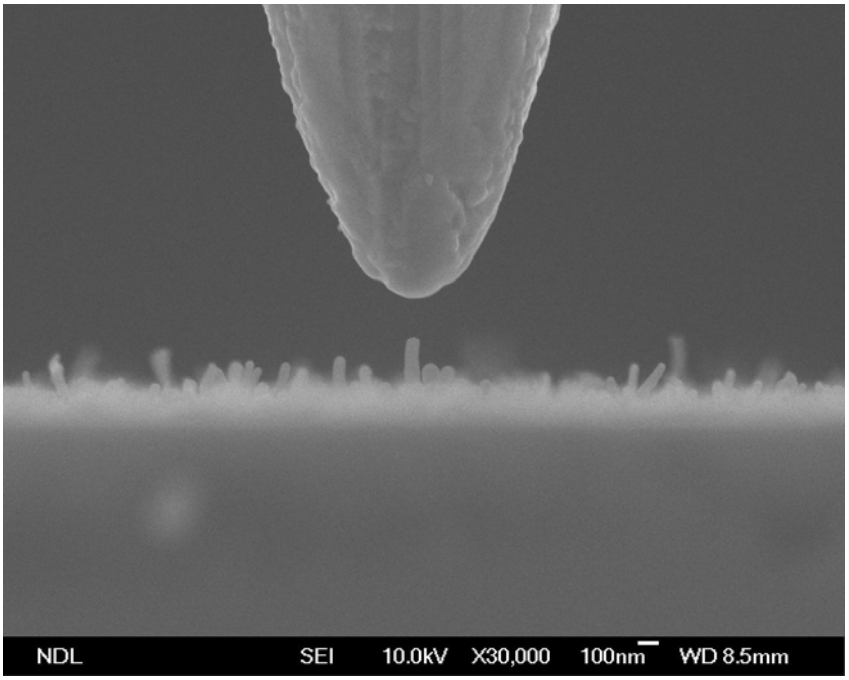

Figure 5-8 *SEM image of a tungsten probe kept at a distance of 300 nm above a 400 nm-long PTCDA nanofiber.*

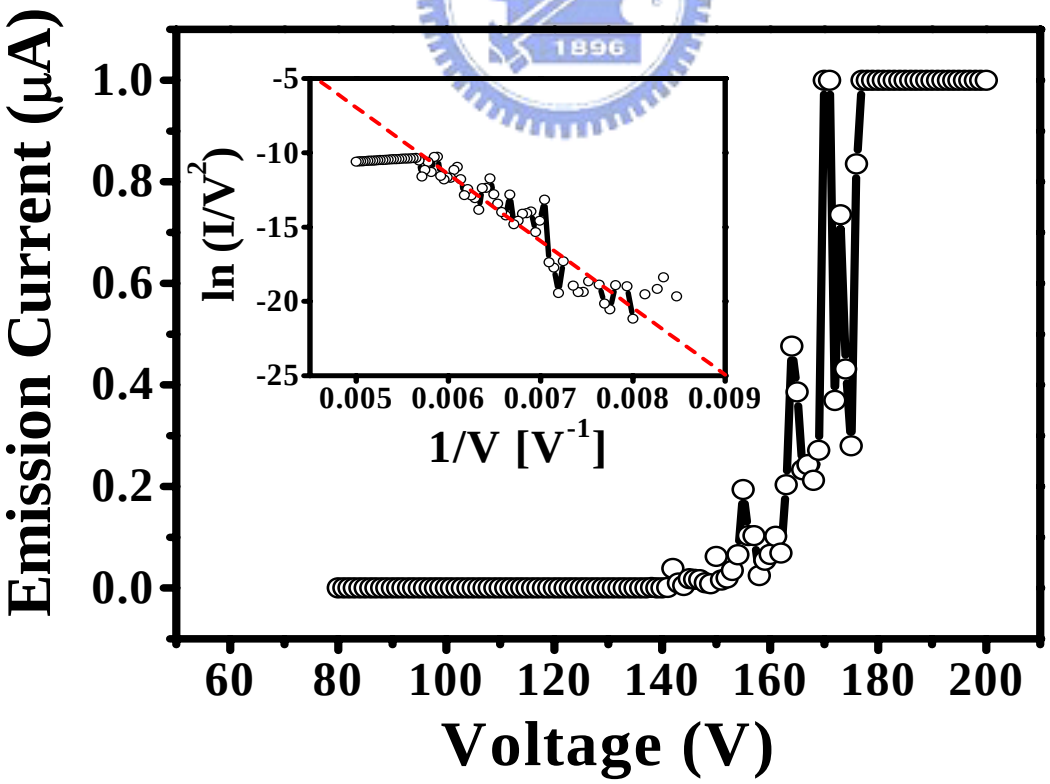

Figure 5-9 *Field emission J–E curve of single PTCDA nanofiber. Inset: Corresponding FN plot.*

Although The turning point is higher than the result of CNTs, i.e. 115 V measured by keeping anode at a distance of 1.25 μm [173], it is much smaller than 205 V, the value of single individual PAH-CNF. From the point of view of electron injection, the work function (4.33 eV) of the Ti substrate [171] is lower than the electron affinity (4.6 eV) of PTCDA [170]; thus, electrons are more readily to give away from the Ti metal. In addition, since PTCDA has a higher electron affinity, the electrons are fond to transfer from Ti to PTCDA. Although the energy barrier between an Au substrate (5.1 eV) to PAH-CNF nanofibers (5.0 eV) is only 0.1 eV, the tiny higher work function of Au still needs an extra energy to overcom the barrier and inject the electrons to the PAH-CNFs film. Furthermore, the strong bonding between the Ti substrate and the dianhydride groups of PTCDA molecules provides a better interface for electron injection [167]. As for PAH-CNFs film, only van der Waals force functioned at the interface; thus a poorer interface leads to a higher field to inject electrons.

Based on this observation, it is easily to predict that the PTCDA nanofibers film should have a lower turn-on field than the PAH-CNFs film. However, the prediction is against the real results, the turn-on field of PAH-CNFs film (5.4 V/μm) is lower than that of PTCDA nanofibers film(8 V/μm). This should ascribes to the difference of fibers growth oreintation of these two nanofibers films. Comparing Figure 5-5 with Figure 3-1, it is clear to see that PAH-CNFs film shows a better fiber orientation than the PTCDA nanofibers film. Therefore, under the same bias field, the well-orientated PAH-CNFs possesses a more focused electron beam, which results in a higher emission current density at a lower biased field.

5.4 Conclusions

In this study, I observed the temperature-induced morphological changes that occurred to PTCDA on Au, Ti-PVD, and Ti-CVD substrates. Owing to the presence of pillared Ti structures and Ti–Cl reactive sites, PTCDA nanofibers grew much more readily on the Ti-CVD substrate than on the Au and Ti-PVD substrates. A stable emission current was measured when the PTCDA nanofibers were biased under vacuum. The turn-on field required to produce a current density of 10 μA/cm^2 was 8 V/μm; the maximum emission current density was 1.3 mA/cm^2, measured at E = 11 V/μm. From the slope of the straight line obtained after plotting ln (J/E^2) versus 1/E, I calculated the field enhancement factor to be ca. 989 cm^{-1}. These results demonstrate an alternative application of PTCDA as an electron-emitting device and open up an interesting area of study of the anisotropic carrier transfer in 1D organic nanostructure.